URN (Paper): urn:nbn:de:gbv:ilm1-2011iwk-021:3

56TH INTERNATIONAL SCIENTIFIC COLLOQUIUM
Ilmenau University of Technology, 12 – 16 September 2011
URN: urn:nbn:gbv:ilm1-2011iwk:5

ANALYTICAL INVESTIGATIONS AND ADAPTIVE CONTROL OF VIBRISSAE-LIKE SENSOR MODELS WITH FINITE DOF

Tonia Schmitz / Carsten Behn

Department of Technical Mechanics
Ilmenau University of Technology
Max-Planck-Ring 12 (Building F)
98693 Ilmenau, Germany
tonia.schmitz@gmx.de / carsten.behn@tu-ilmenau.de

ABSTRACT

Mice and rats use a sophisticated sensory system to acquire tactile information about their surroundings. Vibrissae, located in the mystacial pad, are either used passively to sense environmental forces, e.g., wind, or actively, when they are rhythmically moved to scan objects or surfaces. Inspired by this biological sensory system, three mechanical models with a rigid, rod-like vibrissa are developed based on findings in the literature. The models take into account the viscoelastic support of the vibrissa in the mystacial pad (follicle-sinus-complex and skin) on the one hand, and on the other hand they simulate the muscles (extrinsic and intrinsic) empowering the animals to whisk actively by using adaptive control algorithms. To model the range of movement of the biological vibrissa, the degree of freedom is gradually increased from 1 to 3 — enabling the examination of the support's influence on the sensitivity of the system. Numerical simulations with chosen perturbation forces show that specific control variables contain adequate information on the force to be identified.

Index Terms— Vibrissa, tactile sensor, mechanical model, adaptive control.

1. INTRODUCTION

Mice and rats use the vibrissae in the mystacial pad (see Fig. 1, left) to acquire informations about their surroundings. While the vibrissa itself, just consisting of dead tissue, is mainly used as a lever for the force transmission, the actual detection of contact forces is made possible by pressure-sensitive mechanoreceptors in the support of the vibrissa – the follicle-sinus-complex (see Fig. 1, right). Each vibrissa has its own follicle-sinus-complex, consisting of the hair follicle embedded in a blood-sinus, ensuring its viscoelastic support. [1; 2]

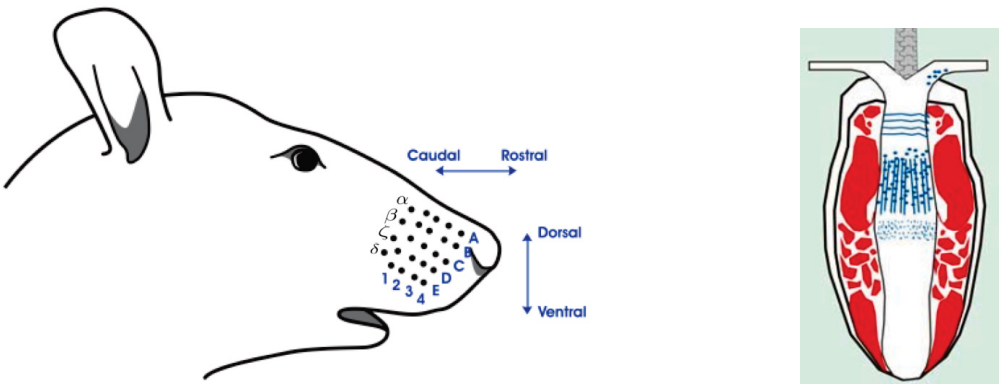

Fig. 1. **Left:** schematic drawing of the mystacial pad. **Right:** schematic drawing of the follicle-sinus-complex consisting of the hair follicle and the blood-sinus (in blue: the mechanoreceptors), [2].

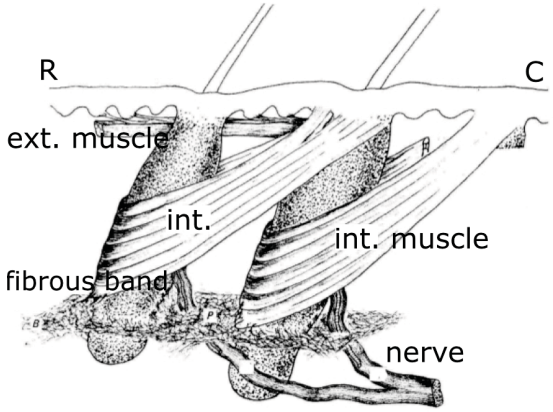

Fig. 2. Schematic drawing of two neighbouring mystacial follicles, which can be moved by extrinsic and intrinsic muscles (latter innervated by the facial nerve). Note that the attachment point of an intrinsic muscle sling is always situated at its neighbouring follicle. (R - rostral, C- caudal) [1]

The vibrissae can either be moved passively (e.g., by wind), or actively through alternate contractions of the intrinsic and extrinsic muscles (see Fig. 2). The resulting rhythmic pro- and retractions of the vibrissae, called whisking, are used to scan surfaces of interest, gathering relevant informations by adjusting the frequency and amplitude of the oscillation to each task. By observing rats accomplishing several types of exercises, Berg and Kleinfeld [3] could distinguish two main **whisking patterns**:

- **exploratory whisking**: rodents explore their environment with large amplitude sweeps in a low frequency (5-15Hz) range,
- **foveal whisking**: rodents palpate object surfaces with small amplitude, high frequency (15-25Hz) movements.

How the animals convert these multiple contacts with single objects into coherent informations about their surroundings remains unclear. However there is the consensus that the position of an object is encoded spatially and temporally – relatively to the initial position of the snout and the vibrissae, [4].
Furthermore, every biological sensory system has the ability to constantly adapt its sensitivity to its current environment in a way that empowers it to distinguish the relevant informations out of the multitude of negligible stimuli (→ *adaptive system*). Several **control strategies** enhance the relevance-oriented stimulus processing:

- a feedback-loop (closed-loop control system) enables the rodents to immediately react to an object contact: they slow down the concerned vibrissae, diminishing the occuring wear-out effect on the hair, [5; 6],
- depending on the mode (passive or active) and the expectations of the rodent, the neurons reaction is being suppressed, enhanced or left unaltered, [7; 8; 9],
- the rodents can probably modify the stiffness of the vibrissa support by varying the pressure in the blood-sinus, [1; 2], and by so doing, specifically alter the properties of the vibrissa in motion.

This biological sensory system is highly interesting for applications in the field of autonomous robotics, since tactile sensors can offer reliable information, where conventional sensors fail – in dark, smoky or noisy environments. Nevertheless the goal of our work is *not* to recreate an exact copy of the biological system, but **to implement in a mechanical model the specific characteristics of the vibrissa needed for the detection of useful informations in challenging surroundings.**

2. STATE OF THE ART

Since R. Andrew Russel, an australian scientist from the University of Wollongong, succeeded in the 1980s to determine the position of a robot arm with vibrissa-like sensors (made of guitar strings) [10], the demand for technical vibrissae grew steadily. Meanwhile tactile sensors often complement or even replace optical sensors in their two main fields of application: flow measurements and autonomous robotics. However especially in the latter field, technical vibrissae are currently just used to avoid imminent collisions: as mere contact sensors with a binary output, [11]. Nevertheless in the last decade, the number of scientific publications in which the skills of the tactile sensors were improved, grew significantly. While it still constituted a considerable achievement in 1996, to just let robots equipped with vibrissae drive along walls, [12], more recently robots with a similar configuration managed to distinguish objects on the basis of their surface texture, [13; 14; 15; 16; 17], or to determine the form and position of nearby objects, [18].

In the majority of the encountered papers, the development of innovative technical whiskers was based on mechanical models of the vibrissa. As the focus of this paper lies on mechanical models with a finite degree of freedom, only models with a rigid, rod-like vibrissa are presented in the following.

2.1. Model of the follicle-sinus-complex

Mitchinson's research group [19; 6] has developed a model of the follicle-sinus-complex (FSC) to increase the knowledge over this biological sensory system on the one hand, and on the other hand to promote the development of innovative and efficient tactile sensors. Following the anatomical descriptions in the literature, the scientists modeled the various layers of the FSC, linking them with spring and damping elements (see Fig. 3) to simulate the compliance of the biological tissue. However, the model has been confined at the level of the ring-sinus, as the density of the mechanoreceptors is believed to be the highest there (also see Fig 1, right) – besides at this level the FSC is nearly symmetrical to its longitudinal axis, so that only a radial section had actually to be taken into account.

In numerical simulations, the model was gradually improved by varying the parameters (damping and spring stiffness, see Tab. 1) until the motion characteristics of the modeled vibrissa fitted those of the biological vibrissa.

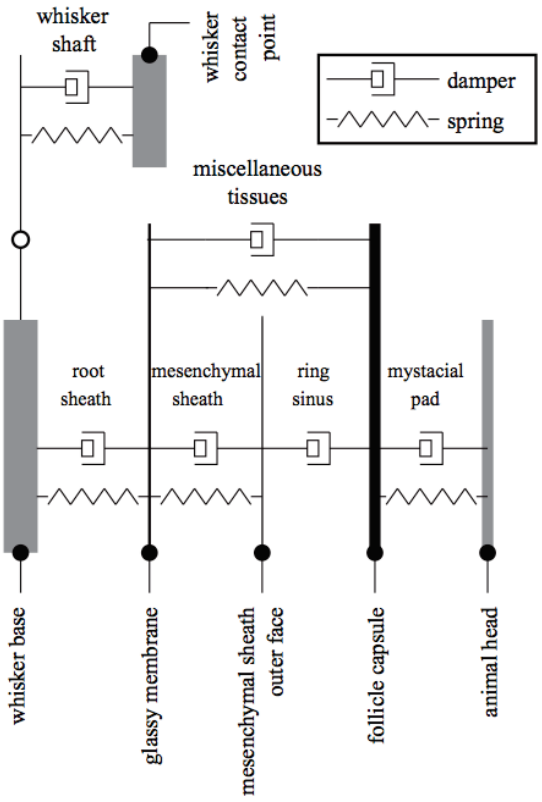

Fig. 3. Mechanical model of the FSC, [19].

Parameter		Value
Spring stiffnes		
estimated	c_{RS}	$5kNm^{-1}$
	c_{MS}	$100kNm^{-1}$
chosen	c_{MP}	$100kNm^{-1}$
	c_{MT}	$50kNm^{-1}$
	c_{WS}	$100kNm^{-1}$
Damping		
estimated	d_{RS}	$2\sqrt{m_{GM}k_{RS}}Nsm^{-1}$
	d_{MS}	$2\sqrt{m_{MSO}k_{MS}}Nsm^{-1}$
	d_{MT}	$2\sqrt{m_{GM}k_{MT}}Nsm^{-1}$
	d_{WS}	$2\sqrt{m_{WC}k_{WS}}Nsm^{-1}$
	d_{MP}	$2\sqrt{m_{FC}k_{MP}}Nsm^{-1}$
	d_{SI}	$2\sqrt{m_{GM}k_{RS}}Nsm^{-1}$

Table 1. Parameters: RS - root sheat, MS - mesenchymal sheath, MT - miscellaneous tissues, WS - whisker shaft, MP - mystacial pad, SI - ring sinus; [19].

2.2. Model of the musculature in the mystacial pad

The function of the musculature in the mystacial pad was investigated by Berg and Hill in [3; 20]. The scientists recorded electromyogram (EMG) activity from the intrinsic and extrinsic muscles while rats were whisking, to characterize the pattern of muscular dynamics. The following observations were made during one whisking cycle (also see Fig. 4):

- the **protraction** of the vibrissa is caused by the contraction of the intrinsic muscle retracting the FSC (→ **angular deflection**),

- the **retraction** of the vibrissa is induced by the contraction of the extrinsic muscle retracting the vibrissa at skin level (→ **translatory shift**).

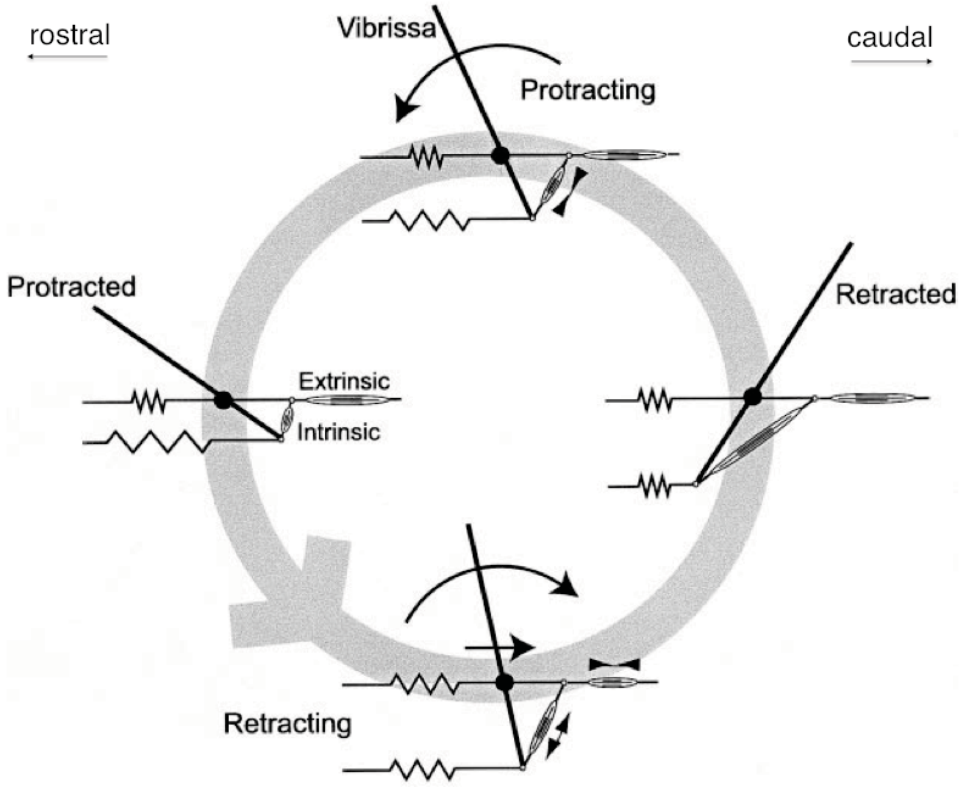

Fig. 4. Mechanical model relating cyclic vibrissa movements to the alternating intrinsic and extrinsic muscle contractions during whisking, [3].

In the resting position, the angle between the vibrissa and the snout amounts to $\varphi_{rest} \approx 80°$. While whisking, the vibrissa is being protracted to an angle of $\varphi_{rest} + 65°$ and retracted to an angle of $\varphi_{rest} - 35°$. In addition, during whisking the pivot point of the vibrissa (located at skin level) slides up to $\sim 5mm$ in the caudal-rostral direction and up to $\sim 3mm$ in the dorsal-ventral direction. These observations imply that the total range of movement of the vibrissa can only be attained due to the interaction of the different types of musculature. Based on these findings, the researchers developed a mechanical model of the vibrissa, focussing on the relationship between the various muscle contractions and the resulting vibrissa motion. Furthermore three vibrissa / follicle units, linked by spring and damping elements, were incorporated in the model so that the influence of the intrinsic muscle slings on their neighbouring follicles could also be considered, (see Fig. 5 with Tab. 2).

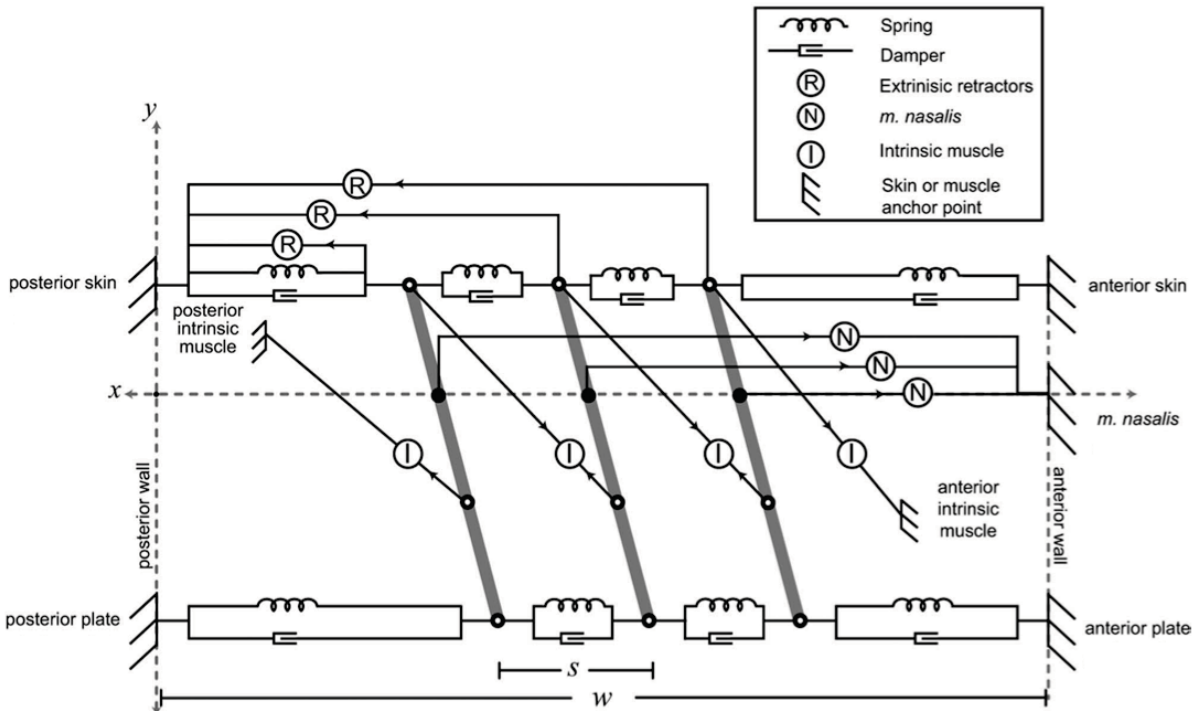

Fig. 5. Schematic drawing of the mechanical model of a row of three vibrissae, [20].

Description	**Parameter**	**Value**
Number of vibrissae	N	3
Length of hair	l_h	40mm
Length of follicle	l_f	4mm
Distanz between vibrissae at rest	s	2mm
Extent of mystacial pad	w	20mm
Resting angle of vibrissae	ϕ_{rest}	80
Mass of hair	M_h	0.5mg
Masse of follicle	M_f	10mg
Center of mass of vibrissa as measured from base of hair	C	-1.43mm
Moment of inertia of vibrissa unit about center of mass	I	112mg·mm^2
Relaxation time-constant of the mystacial pad	$\tau_{Rel.}$	27ms

Table 2. Parameters used in simulations, [20].

The parameters in Table 2 were used to calculate the spring and damping constants of the mystacial pad. The fact that a passively deflected vibrissa returns to its initial position without oscillating, implies that the mystacial pad is overdamped, [20], thus equation (1) describes the relationship between the spring (c) and damping (d) coefficients. A multiplication factor of 4 was arbitrarily chosen because of the relative insensitivity of a linear overdamped system to the exact value of this ratio:

$$\begin{aligned} & \frac{d^2}{4c} > N \cdot (M_h + M_f) \\ \Rightarrow \quad & \frac{d^2}{4c} = 4N \cdot (M_h + M_f). \end{aligned} \tag{1}$$

The spring and damping constants of the mystacial pad were determined using equation (2) with the relaxation time constant ($\tau_{Rel.}$) and the measured masses of the hair (M_h) and the follicle (M_f) (see Tab. 2):

$$\begin{aligned} \tau_{Rel.} &= \frac{2N(M_h + M_F)}{d - \sqrt{d^2 - 4cN(M_h + M_f)}} \\ \xrightarrow{(1)}\ \tau_{Rel.} &= \frac{2N(M_h + M_F)}{d - \sqrt{d^2(1 - \frac{1}{4})}} = \frac{2N(M_h + M_F)}{d\big(1 - \sqrt{\frac{3}{4}}\big)}, \end{aligned} \tag{2}$$

$$d = \frac{2N(M_h + M_F)}{\tau_{Rel.}\big(1 - \sqrt{\frac{3}{4}}\big)} = 17.41\left[\frac{Ns}{m}\right], \qquad c = \frac{d^2}{4 \cdot 4N \cdot (M_h + M_f)} = 601.8\left[\frac{N}{m}\right].$$

2.3. Model of the stimulus transmission from the vibrissa to the mechanoreceptors

Based on mechanical models and control algorithms presented by Behn and Steigenberger in [21; 22; 23], an abstract model of the stimulus transmission from the vibrissa to the mechanoreceptors was developed by Schmitz in [24]. The system has been divided into the two levels of stimulus reception (vibrissa) and stimulus processing[1] (mechanoreceptors) to assign an appropriate model to each.

Fig. 6. Model of the stimulus transmission from the vibrissa to the mechanoreceptors. $\vec{F}(t)$ - input signal (disturbing force), $\vec{M}_u(t)$ - control torque, α - dimensional factor, $y(t)$ - output signal, [24].

2.3.1. Vibrissa model

The level of stimulus reception was simulated with a mechanical model containing essential characteristics of the biological vibrissa (see Fig. 7). The center of rotation of the thin, rod-like vibrissa lies at skin level, a viscoelastic element located beneath it, represents the compliance of the FSC.

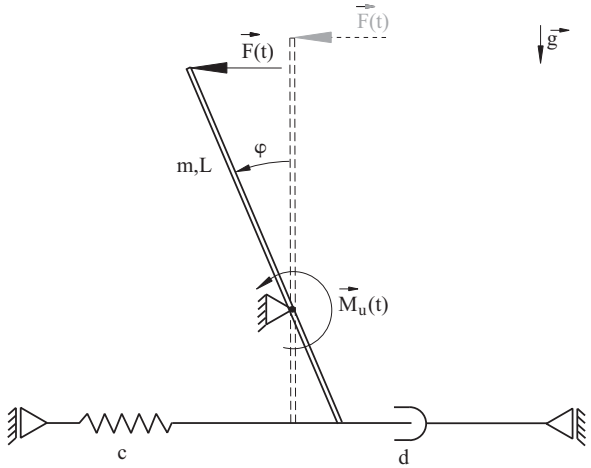

Fig. 7. Mechanical model of the vibrissa: d - viscous damping coefficient, c - spring constant, m - mass of the rod, L - length of the rod, $\vec{F}(t)$ - disturbing force, $\vec{M}_u(t)$ - control torque, [24].

[1] Although the actual processing of the stimuli takes place in the rodents brain, the mechanoreceptors play an important role in the selection of the significant informations. [25]

The ability of the rodents to either stabilise or swing their vibrissa actively, was implemented with a control torque $\vec{M}_u(t)$. The differential equation (3) describes the motion of the rod:

$$\ddot{\varphi}(t) = \frac{1}{J_{0z}}\left[\left(L - \frac{L}{a}\right)F(t)\cos(\varphi(t)) - c\frac{L^2}{a^2}\cos(\varphi(t))\sin(\varphi(t)) - d\frac{L^2}{a^2}\cos^2(\varphi(t))\dot{\varphi}(t) + \left(\frac{L}{2} - \frac{L}{a}\right)mg\sin(\varphi(t)) + M_u(t)\right], \quad (3)$$

with the following initial conditions:

$$\varphi(0) = 0 \qquad \dot{\varphi}(0) = 0,$$

and the control algorithm (developed in [21; 22; 23]) generating the torque $Z_u(t) = M_u(t)$ with $z = \varphi$:

$$\left.\begin{aligned} e(t) &:= z(t) - z_{refi}(t) \\ Z_u(t) &= -\left[k(t)e(t) + \kappa\big(k(t)\dot{e}(t)\big)\right] \\ \dot{k}(t) &= \begin{cases} \gamma(||e(t)|| - \lambda)^2, & \text{when } ||e(t)|| \geq \lambda + 1 \\ \gamma(||e(t)|| - \lambda)^{0,5}, & \text{when } (\lambda + 1) > ||e(t)|| \geq \lambda \\ 0, & \text{when } (||e(t)|| < \lambda) \wedge (t - t_E < t_d) \\ -\sigma k(t), & \text{when } (||e(t)|| < \lambda) \wedge (t - t_E \geq t_d) \end{cases} \end{aligned}\right\} \forall t. \quad (4)$$

The gain factors of the control algorithm were set to: $\sigma > 0$, $\kappa = 1$ and $\gamma \gg 1$. The reference signal $z_{refi}(t)$ (with $i = 0, 1$) simulates the passive mode when set to $z_{ref0}(t) = 0$, and the active mode when for example set to $z_{ref1}(t) = \frac{\pi}{8}\sin(5t)$. The margin of tolerance was set to $\lambda > 0$ and the dwell time to $t_d = 2$. t_E is an internal parameter.
When an external force deflects the rod, the gain factor k increases until the deflection $\varphi(t)$ enters the λ-tube, dwells in there for the time t_d and decreases afterwards with $-\sigma k(t)$. The constant adaption of the gain factor ensures the high sensibility of the system, since a new disturbance force can only be percieved, if the generated torque $\vec{M}_u(t)$ allows a sudden, additional deflection. Furthermore the influence of the measured error e is being taken into account: the control algorithm distinguishes between great and small error values and enables good system dynamics in both cases.
Thereby the control algorithm (4) has the ability to compensate *unknown* disturbance forces in the passive, as well as in the active mode: the rod-like vibrissa follows the reference signal (φ_{ref}, see Fig. 8) within the margin of tolerance λ. This is similar to the rodents reaction: they suppress the perception of a *bothering* permanent vibrissa deflection (here: keeping the motion of the rod in the λ-tube), while still staying sensitive for an *interesting* sudden deflection.

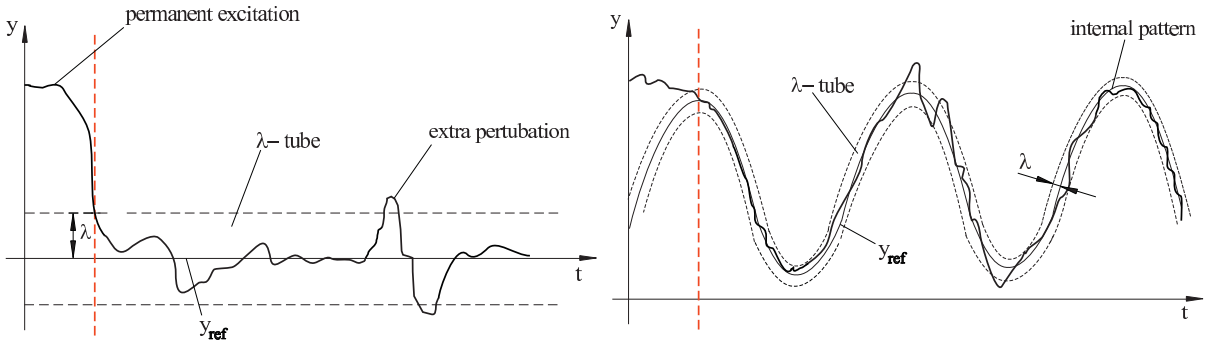

Fig. 8. Left: passive mode (λ- stabilisation), right: active mode (λ-tracking), [26].

2.3.2. Receptor model

The mechanoreceptors were modeled as a mass-spring-damper system in a box (depicted in Fig. 9) with an indirect excitation over the control torque $\vec{M}_u(t)$ generated in the vibrissa model. An additional control force $\vec{u}(t)$ stabilizes the mass oscillations and thus simulates the ability of the mechanoreceptors to constantly adapt their sensibility to the actual situation: *suppressing* the annoying persisting stimuli and *enhancing* the interesting sudden stimuli.

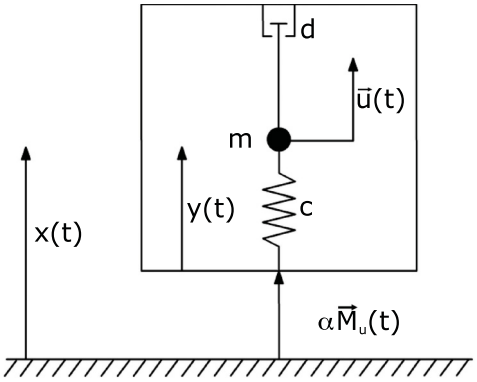

Fig. 9. Mechanical model of the mechanoreceptors; d - viscous damping coefficient, c - spring constant, m - seismic mass, $\vec{u}(t)$ - control force, $x(t)$ - absolute coordinate, $y(t)$- relative coordinate, $\vec{M}_u(t)$- control torque generated in the vibrissa model, α - dimensional factor; [21].

The differential equation (5) describes the motion of the mass in the receptor model:

$$\ddot{y}(t) = -\frac{d}{m}\dot{y}(t) - \frac{c}{m}y(t) + \frac{1}{m}u(t) - \alpha \cdot M_u(t), \tag{5}$$

with the dimensional factor $\alpha \geq 1$ and the initial conditions:

$$\begin{aligned} y(0) &= x_0 - \varphi(0), & x_0 &= 0, \\ \dot{y}(0) &= x_1 - \dot{\varphi}(0), & x_1 &= 0. \end{aligned}$$

The control force $\vec{u}(t)$ is being generated by the algorithm (4) with $z = y$ and one single reference signal $z_{ref}(t) = 0$, as the mass motion only needs to be stabilized at its rest position.

2.3.3. Performance of the model

In numerical simulations with *MATLAB* (version 7.6), several external forces (e.g., approximated gust of wind, encounter with an object) have been used to examine the performance of the vibrissa-receptor-model, especially regarding its sensibility and adaptivity. Altogether the vibrissa model is sensitive and reacts well to the external forces: the vibrissa can be stabilized and actively moved due to the control torque $\vec{M}_u(t)$. Moreover the disturbing force can clearly be recognized in the course of the control torque, which thereby has been found suitable for the use as an input signal for the receptor-model. This model is able to rapidly suppress the persisting stimuli and shows a good reaction to sudden deflections. The external force (occuring at the tip of the vibrissa) can be identified with the plots of the displacement $y(t)$ and the reaction of the control force $\vec{u}(t)$ in the receptor model.

2.4. Brief summary

Table 3 summarizes the relevant informations found in the literature for this paper.

Mechanical models with a stiff vibrissa	
Mitchinson 2004, 2007	**Model of the follicle-sinus-complex**
[19; 6]	⊖ too complex for a technical implementation
	⊕ Determinantion of spring and damping coefficients for the FSC
Berg 2003, Hill 2008	**Model of the musculature in the mystacial pad**
[3; 20]	⊕ Implementation of the intrinsic and extrinsic musculature
	⊕ Simulating the viscoelastic properties of the skin ↪ Determination of spring and damping coefficients for the skin
	⊖ Neglect of the viscoelastic properties of the FSC
	⊖ Connection between the follicles ↪ leads to complex control strategy
	Determination of the range of movement of the vibrissa
	↪ $\varphi_{Rest} \approx 80°$
	angular deflection in rostral direction $\varphi_{Rest} + 65°$
	angular deflection in caudal direction $\varphi_{Rest} - 35°$
	translatory shift $\approx 5mm$ in caudal-rostral direction
	translatory shift $\approx 3mm$ in dorsal-ventral direction
Schmitz 2009	**Model of the stimulus transmission**
Behn 2005, 2009	⊕ Implementation of the viscoelastic properties of the FSC
[24; 21; 22; 23]	⊖ Neglect of the viscoelastic properties of the skin
	⊕ Simulation of the passiv/active mode ↪ through adaptive control algorithms

Table 3. Summary of the state of the art with a brief evaluation of the model characteristics with respect to the development of improved models, (⊕: positive feature, ⊖: negative feature).

3. DEVELOPING VIBRISSA MODELS WITH A FINITE DEGREE OF FREEDOM

Starting from the publications presented in Section 2, three innovative mechanical models with a stiff, rod-like vibrissa are being developed, (see Fig. 10). The degree of freedom (DoF) is being successively increased from 1 to 3, to investigate the impact of different supports on the sensory capabilities of the system.

- In **model 1** the rod has one rotational degree of freedom: the angular deflection $\varphi(t)$. The control torque $\vec{M}_u(t)$ simulates the rodents ability to regulate the deflection of the vibrissa with their intrinsic musculature.
- In **model 2A** the rod has, in addition to the rotational, a linear degree of freedom: the lateral translatory motion of the pivot point (following the informations found in [20; 3], see Subsection 2.2). A control force $\vec{F}_{ux}(t)$ simulates the rodents ability to alter the position of the pivot point through contractions of the extrinsic musculature.
- In **model 2B** the rod has two degrees of freedom as well: the angular deflection as in the models 1/2A and a longitudinal translatory motion of the vibrissa. A control force $\vec{F}_{uy}(t)$ determines the longitudinal position of the pivot point. This force is not simulating any natural musculature, see Remark 3.1.
- In **model 3** the models 2A and 2B are being combined, thus the rod possesses three degrees of freedom, which enables it to perform a rotatory deflection, as well as lateral and longitudinal displacements.

Remark 3.1. *The implementation of the linear degree of freedom in the longitudinal direction is based on findings in [27], revealing that vibrissa experience considerable forces in longitudinal direction when touching an object. Furthermore Stuettgen [28] found out that the rodents neurons react strongly to the*

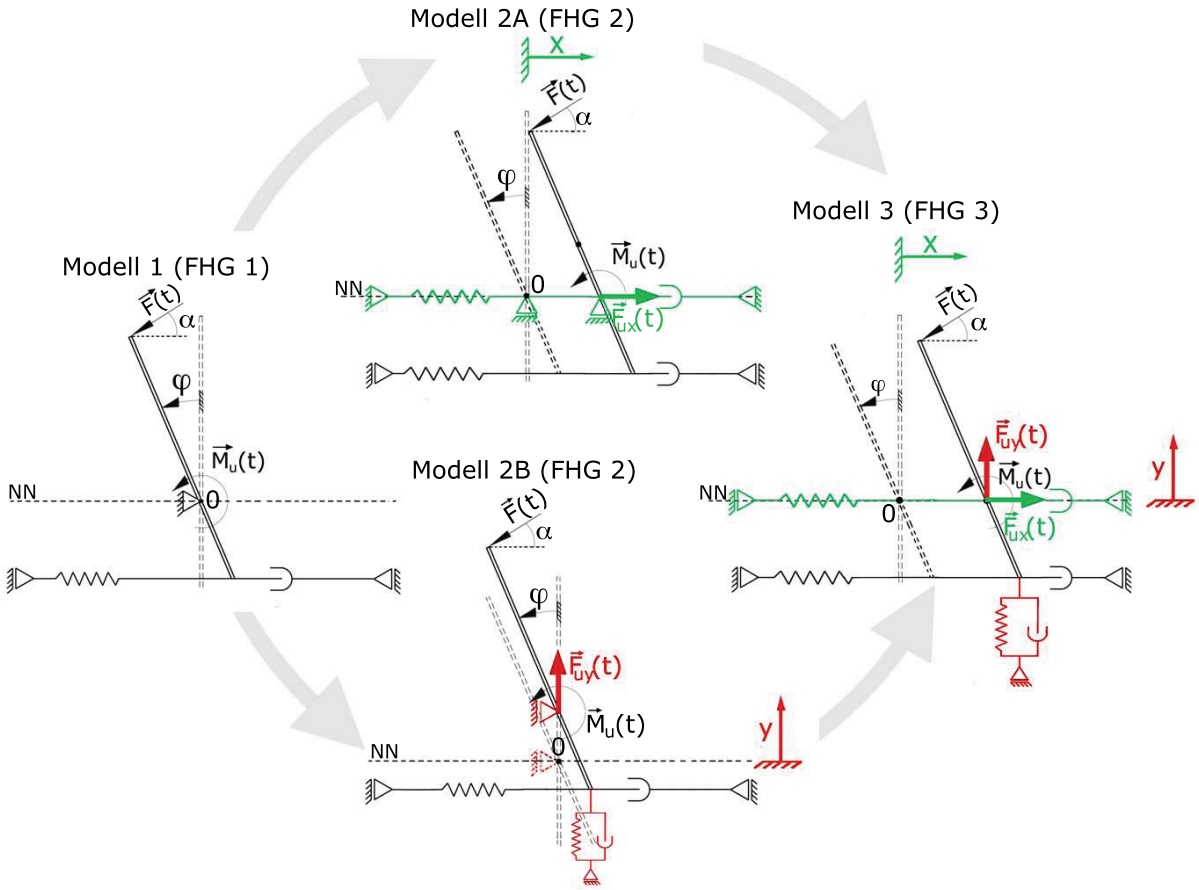

Fig. 10. Innovative mechanical models with a rigid, rod-like vibrissa, (x: lateral direction, y: longitudinal direction).

longitudinal displacements of the vibrissa – which leads to the assumption that they provide relevant informations about their environment.

	Model 1	**Model 2A**	**Model 2B**	**Model 3**
Compliance of the skin		√		√
Lateral compliance of the FSC	√	√	√	√
Longitudinal compliance of the FSC			√	√
Torque $\vec{M}_u(t)$	√	√	√	√
Force $\vec{F}_{ux}(t)$		√		√
Force $\vec{F}_{uy}(t)$			√	√

Table 4. Summarizing list of the characteristics and the control variables implemented in the different models.

The models are all equipped with a rod of the length L, supported at a height a, performing a rotational deflection $\varphi(t)$ when an external force $\vec{F}(t)$ touches its tip. A spring-damper-element beneath the pivot point simulates the lateral compliance of the FSC. The angular deflection of the rod is being controlled by a torque $\vec{M}_u(t)$ generated by the control algorithm (4) already presented in Subsection 2.3.

In the passive mode, the rod motion only needs to be stabilized, therefore it can be simulated with the reference signal (6). The active mode has to be implemented with reference signals performing periodical oscillations

enabling the rod to either explore its surroundings or to scan specific objects – and since rodents use two different kinds of oscillations depending on the task, the exploratory and foveal whisking are simulated by two different reference signals. Rodents employ large amplitude sweeps in a low frequency range (5-15Hz) to investigate their environment. As the range of movement of the biological vibrissa amounts to ca. $100^\circ = 1.74$ rad (see Subsection 2.2), the amplitude of the exploratory reference signal (7) can be chosen to $A = \frac{1.74}{2} \approx 0.8$ rad. The frequency of the signal $\varphi_{ref1}(t)$ has been set to $f = 5$ Hz according to the findings in [3]. Foveal whisking has been implemented with the reference signal (8), using an amplitude of $A = 0.2$ rad $\approx 12^\circ$ and a frequency of $f = 25$ Hz, since rodents scan specific objects with small amplitude, high frequency movements ($15 - 25$ Hz).

$$z_{ref0}(t) = \varphi_{ref0} = 0 \tag{6}$$
$$z_{ref1}(t) = \varphi_{ref1} = 0.8\sin(5t) \tag{7}$$
$$z_{ref2}(t) = \varphi_{ref2} = 0.2\sin(25t) \qquad \forall t \tag{8}$$

The additional control forces $\vec{F}_{ux}(t)$ (for the models 2A and 3) and $\vec{F}_{uy}(t)$ (for the models 2B and 3) needed to stabilize the lateral or longitudinal displacements of the rod, are also being generated by the algorithm (4), although with the reference signals $z_{ref0}(t) = x_{ref0}(t) = 0$, respectively $z_{ref0}(t) = y_{ref0}(t) = 0$.

Since the characteristics of a system are significantly influenced by the choice of its parameters, it can be advantageous when modeling a biological system to employ the biological values as model parameters. However the characteristic values of a biological system usually vary from animal to animal, as demonstrated in Table 5 with the values of the vibrissa C2 (see Fig. 1, left) measured on different rats (in different publications) – although the order of magnitude between the length/mass of the vibrissa and follicle seems to be roughly consistent.

Source	**Parameter**		
	L – Length of vibrissa	a – Length of follicle	m – Mass of vibrissa
Hill, [20]	$40\,mm$	$4\,mm$	$0.5\,mg$
Neimark, [29]	$37\,mm$	–	$0.291\,mg$
Carl, [2]			
Ratte 1	$33\,mm$	$2\,mm$	$0.267\,mg$
Ratte 2	$23\,mm$	$2\,mm$	–

Table 5. Parameter values of several biological vibrissae C2.

Other values like the viscosity and elasticity of the FSC could not be found in the literature and had to be calculated using the informations in [19] (see Fig. 3 and Tab. 1) with the following assumptions:

1^{st} assumption: $d_i = 0$

$$\frac{1}{\overline{c}} = \frac{1}{c_{MP}} + \frac{1}{c_{MT}} + \frac{1}{c_{RS}} \qquad \rightarrow \overline{c}_{FSC_{lat.}} = 4347\frac{N}{m}$$

2^{nd} assumption: $c_i = 0$

$$d_{//} = \left(\frac{1}{d_{MS}} + \frac{1}{d_{MP}}\right)^{-1} + d_{MT}$$
$$\frac{1}{\overline{d}} = \frac{1}{d_{MP}} + \frac{1}{d_{//}} + \frac{1}{d_{RS}} \qquad \rightarrow \overline{d}_{FSC_{lat.}} = 0.53\frac{Ns}{m}$$

The compliance of the skin can be calculated with the formulas (9) (also see Subsection 2.2 and [20]). With a relaxation time constant $\tau_{Rel.} = 27ms$ and a chosen mass of $0.3mg$, the damping constant amounts to

$d_{skin} = 0.165\frac{Ns}{m}$ and the spring constant to $c_{skin} = 5.671\frac{N}{m}$:

$$d_{skin} = \frac{2m}{\tau_{Rel.}\left(1 - \sqrt{\frac{3}{4}}\right)} = 0.165\frac{Ns}{m}, \qquad c_{skin} = \frac{d_1^2}{16 \cdot m} = 5.671\frac{N}{m}. \tag{9}$$

Since no informations about the longitudinal viscoelasticity of the FSC were available, the parameters $c_{FSC_{long.}}$ and $d_{FSC_{long.}}$ were chosen identical to the lateral spring and damping coefficients of the FSC.

Table 6 summarizes and compares the biological values with the model parameters ascertained in preliminary numerical studies in which the behavior of the four models were analysed and gradually improved by varying the values. The resulting parameter configuration, presented on the right side of Table 6, is being used for all further simulations.

	Parameter		**Biological values**	**Num. sim.**
All models	Vibrissa length	L	$37\,mm$	$40\,mm$
	Follicle length	a	$2\,mm$	$\frac{L}{3}\,mm$
	Vibrissa mass	m	$0.3\,mg$	$1\,mg$
	Lateral spring coefficient of FSC	c_1	$4350\,\frac{N}{m}$	$80\,\frac{N}{m}$
	Lateral damping coefficient of FSC quer	d_1	$0.5\,\frac{Ns}{m}$	$0.5\,\frac{Ns}{m}$
Models 2A & 3	Spring coeff. skin	c_2	$0.2\,\frac{N}{m}$	$80\,\frac{N}{m}$
	Damping coeff. skin	d_2	$5.7\,\frac{Ns}{m}$	$0.5\,\frac{Ns}{m}$
Models 2B & 3	Longitudinal spring coeff. of FSC	c_3	$4350\,\frac{N}{m}$	$80\,\frac{N}{m}$
	Longitudinal damping coeff. of FSC	d_3	$0.5\,\frac{Ns}{m}$	$0.5\,\frac{Ns}{m}$

Table 6. Model parameters, on the left: parameter values found in rodents, on the right: appropriate values for the models, chosen after numerical simulations.

4. SENSORY CAPABILITIES OF THE MODELS

Three types of disturbing forces (see Fig. 11) were used in numerical simulations with *MATLAB* (version 7.6), to analyse and compare the sensory capabilities of the four models:

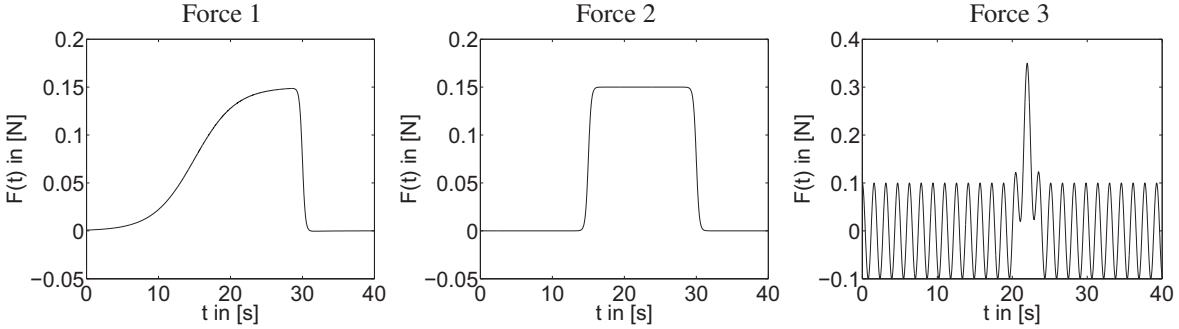

Fig. 11. Disturbance forces used in the num. simulations - left: $\vec{F}_1(t)$, center: $\vec{F}_2(t)$, right: $\vec{F}_3(t)$.

- 1^{st} force: passing by an object

$$F_1(t) = \frac{0.15}{1 + e^{-0.35(t-15)}} - \frac{0.15}{1 + e^{-5(t-30)}}\,[N] \tag{10}$$

- 2^{nd} force: a sudden gust of wind

$$F_2(t) = \frac{0.15}{1 + e^{-5(t-15)}} - \frac{0.15}{1 + e^{-5(t-30)}}\,[N] \tag{11}$$

- 3^{rd} force: texture caracteristics (e.g. roughness) of an object with a single defect

$$F_3(t) = 0.1\cos(4t) + 0.25e^{-(t-22)^2}\,[N] \tag{12}$$

The angle of attack has been varied from $\alpha_0 = 0°$ to $\alpha_2 = 90°$ to investigate its impact on the sensitivity of the system.

However, to limit the content of this paper to its essential results, we chose to only present in detail the models 1 and, in particular 2B – the most promising model. For further informations about the models 2A and 3, see [30].

4.1. Model 1

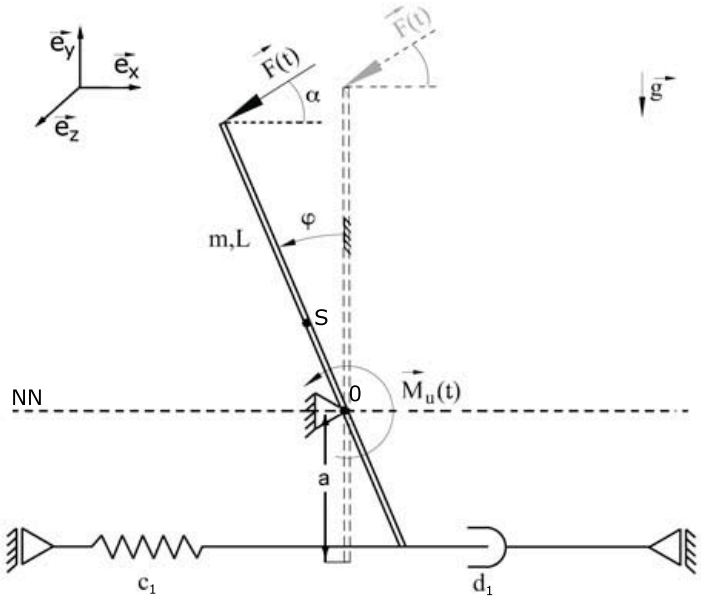

Fig. 12. Vibrissa model 1 (DoF 1): m - mass of the rod, L - rod length, a- follicle length, d - damping coeff., c - spring coeff., $\vec{F}(t)$ - deflecting force, α - angle of attack, $\vec{M}_u(t)$ - control torque. Adapted from [24]

To analyse the sensory properties of the model (see Fig. 12), it is being implemented in *MATLAB* using the differential equation (13), describing the trajectory of the rod:

$$\ddot{\varphi}(t) = \frac{1}{J_{0z}}\Bigg[- d_1 a^2 \cos^2(\varphi(t))\dot{\varphi}(t) - c_1 a^2 \sin(\varphi(t))\cos(\varphi(t)) + mg\left(\frac{L}{2} - a\right)\sin(\varphi(t)) + M_u(t) + (L-a)F(t)\cos(\varphi(t) - \alpha)\Bigg], \tag{13}$$

with the initial conditions:

$$\varphi(0) = 0 \qquad\qquad \dot{\varphi}(0) = 0.$$

Equation (13) has been derived by using the Lagrangean equations of the 2^{nd} kind for this system. To keep the focus of this paper on the sensory capabilities of the models, the derivation of the equation is not being presented, see [30] for a detailed description of the mathematical approach.

In the following, the systems behavior when deflected by an external force is being analysed in the passive and active mode, based on the plots of the rod deflection $\varphi(t)$ and of the control torque $\vec{M}_u(t)$.

4.1.1. Passive mode

Figure 13 depicts the reaction of model 1 when deflected by the 2^{nd} force (11) in the passive mode. The deflection of the rod $\varphi(t)$ is delimited by the control algorithm to the angle of $0.1rad$, so that merely the temporal extension of the acting force can be determined out of its graphical course. However the curve of the torque $\vec{M}_u(t)$ distinctly reproduces the curve of the acting external force for small and medium angles. Furthermore the torque illustrates the decreasing sensitivity of the model for increasing angles of attack. In model 1 only the x-component of the disturbing force leads to a deflection – since this component amounts to zero for $\alpha_2 = 90°$, model 1 is incapable of sensing vertical forces.
Numerical simulations with the 1^{st} and 3^{rd} force (shown in [30]) confirm these statements.

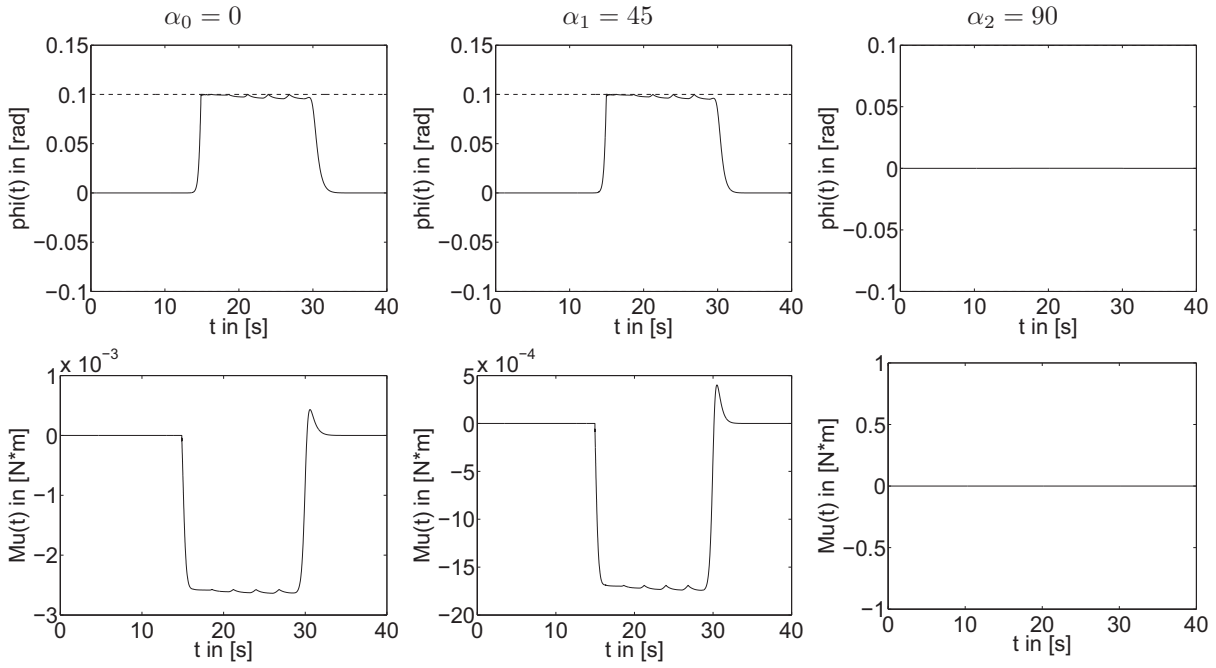

Fig. 13. **Model 1: system behaviour in the passive mode** deflected by the external force $\vec{F}_2(t)$ with different angles of attack α.

4.1.2. Active mode

Figure 14 illustrates the systems reaction in the active mode to the 2^{nd} force as well. In addition to the rather uninformative plots of the deflection $\varphi(t)$, the curves of the error value $e_\varphi(t) := \varphi(t) - \varphi_{ref}(t)$ are being shown – although they are not offering any relevant information either. Solely the course of the torque $\vec{M}_u(t)$ allows some conclusions about the acting force: the torque primarily assures the tracking of the reference signal $\varphi_{ref1}(t)$, nevertheless the moment the tip of the rod is being deflected by the disturbing force, the curve reflects its impact. All in all, the systems reaction is also decreasing with increasing angles of attack – even though the torque paradoxically seems to react to a vertical force in the active mode.

This singularity may be caused by the inaccurate representation of the number π in the floating point arithmetic, internally used in *MATLAB*, [31]. In this special case, the perturbation force enters the differential equation (13) with: $F(t)\cos(\varphi(t) - \frac{\pi}{2})$, so that the initial condition $\varphi(0) = 0$ yields: $F(t)\cos(-\frac{\pi}{2})$. In *MATLAB*, this expression is not equal to 0, but only near 0 – with the result that the external force minimally affects the deflection of the rod, impedes the tracking of the reference signal and thus influences the course of the torque.
These observations were also made with the 1^{st} and 3^{rd} force (numerical simulations shown in [30]).

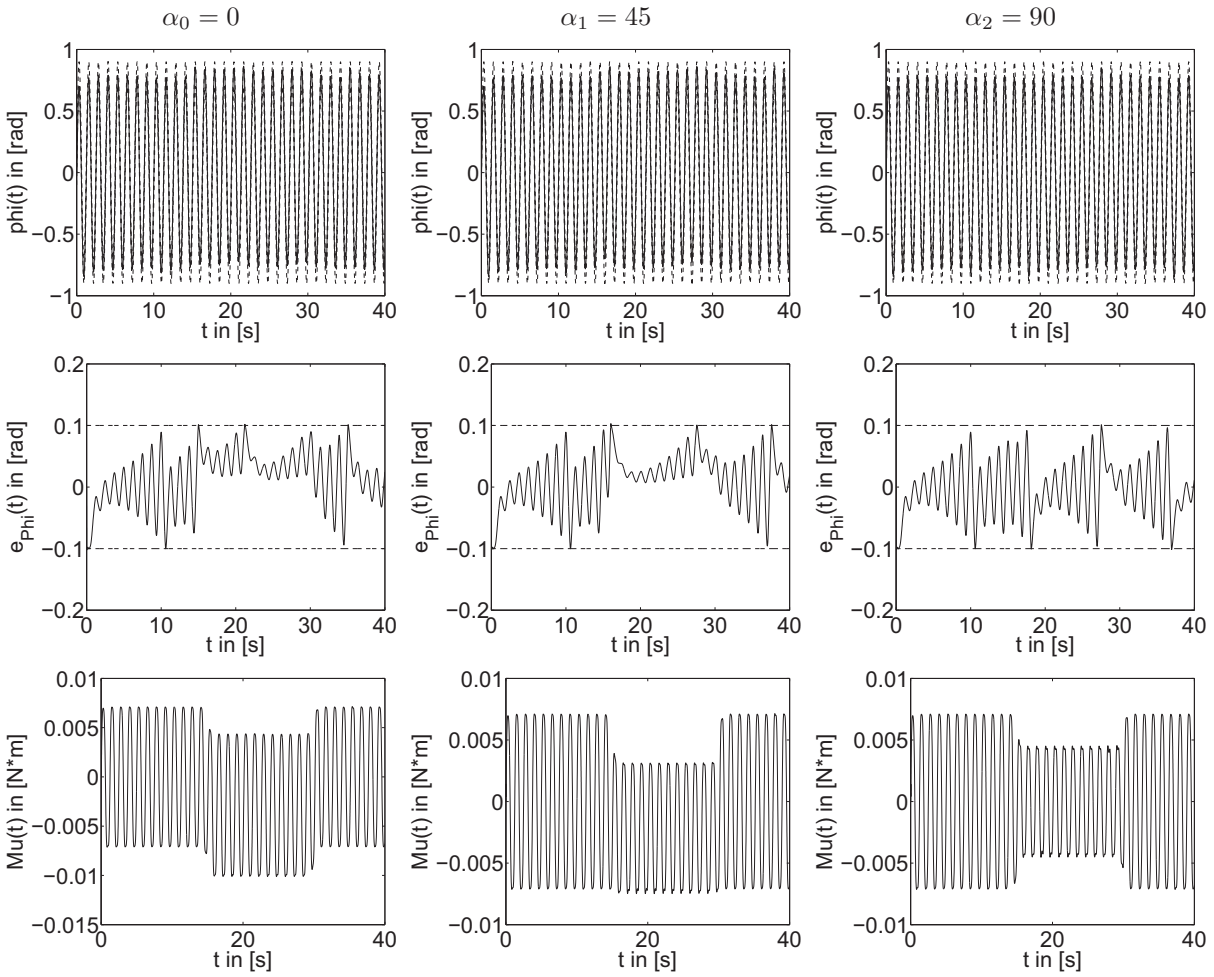

Fig. 14. **Model 1: system behaviour in the active mode** using the reference signal $\varphi_{ref1}(t)$ (exploratory whisking), deflected by the force $\vec{F}_2(t)$ with different angles of attack α.

4.2. Model 2B

The differential equations of model 2B (see Fig. 15), also derived by using the *Lagrangean equations of the* 2^{nd} *kind* (further informations on this approach in [30]), are:

$$\ddot{y}(t) = \frac{1}{m}\Bigg[m\left(\frac{L}{2}-a\right)\left[\ddot{\varphi}(t)\sin(\varphi(t)) + \dot{\varphi}(t)^2\cos(\varphi(t))\right] - d_3\dot{y}(t) - c_3 y(t) - mg \\ - F(t)\sin(\alpha) + F_{uy}(t)\Bigg] \tag{14}$$

$$\ddot{\varphi}(t) = \frac{1}{J_{0z}}\Bigg[m\left(\frac{L}{2}-a\right)\left[\ddot{y}(t)\sin(\varphi(t)) + g\sin(\varphi(t))\right] - d_1 a^2\cos^2(\varphi(t))\dot{\varphi}(t) \\ - c_1 a^2\sin(\varphi(t))\cos(\varphi(t)) + (L-a)F(t)\cos(\varphi(t)-\alpha) + M_u(t)\Bigg] \tag{15}$$

with the initial conditions:

$$y(0) = 0, \qquad \dot{y}(0) = 0,$$
$$\varphi(0) = 0, \qquad \dot{\varphi}(0) = 0.$$

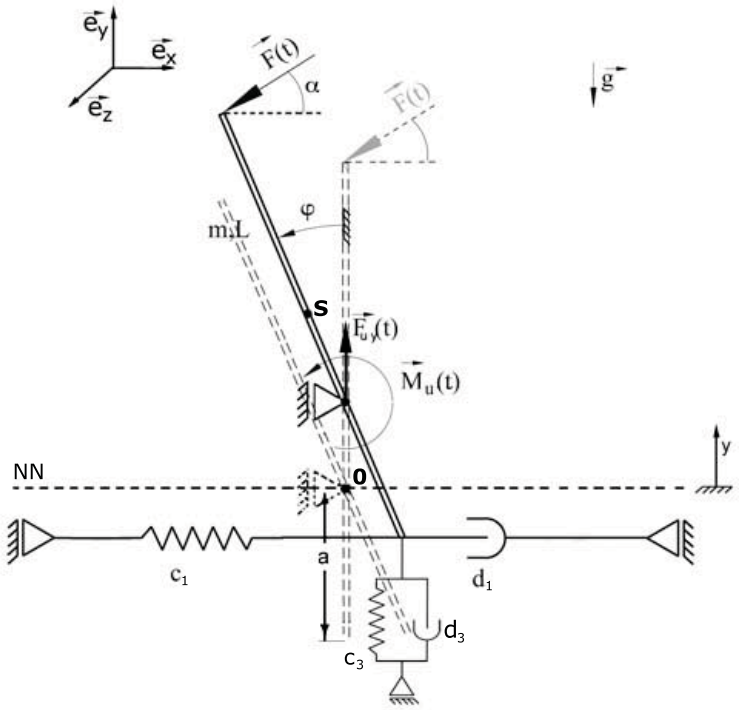

Fig. 15. Vibrissa model 2B (DoF 2): L - rod length, m - mass of the rod, a - follicle length, $d_1,\ d_2$ - damping coeff., $c_1,\ c_2$ - spring coeff., $\vec{F}(t)$ - deflecting force, α - angle of attack, $\vec{M}_u(t)$ - control torque, $\vec{F}_{uy}(t)$ - longitudinal control force.

In this model, the external force $\vec{F}(t)$ does not only induce a rotational, but also a longitudinal translatory displacement of the rod. In the following, the angular deflection will be analysed based on the plots of the rods deflection $\varphi(t)$ and of the control torque $\vec{M}_u(t)$. The translatory motion is being examined using the plots of the displacement $y(t)$ and of the control force $\vec{F}_{uy}(t)$. The graphs have been arranged according to their direction of motion, in the active mode the graphs of the rotational deflection $\varphi(t)$ have been left out in favor of the graphs of the error value e_φ.

4.2.1. Passive mode

The Figures 16 and 17 illustrate the systems reaction on the 2^{nd} external force (11) in the passive mode, depending on its angle of attack. The plots of the angular deflection $\varphi(t)$ are identical to the plots out of the simulations with model 1 (see Fig. 13). This leads to the conclusion that the additional DoF in longitudinal direction, does not interfere with the rotational rod motion. Thus, as in model 1, the course of the control torque $\vec{M}_u(t)$ reflects the course of the exerted force for small and medium angles of attack, whereby the sensitivity of the model decreases for increasing angles of attack. A vertical force causes no angular deflection $\varphi(t)$.

The graphs of the translatory displacement $y(t)$ provide a reliable representation of the acting force and this with *increasing sensitivity for increasing angles of attack*. This is due to the fact that only the y-component of the external force leads to a translatory displacement – accordingly horizontal forces ($\alpha = 0°$) cannot be perceived. However the plot of the control force $\vec{F}_{ux}$ gives a disappointingly bad idea of the disturbing force – independently of the angle of attack.

Numerical simulations with the 1^{st} and 3^{rd} disturbing force (shown in [30]) confirm the statements made above.

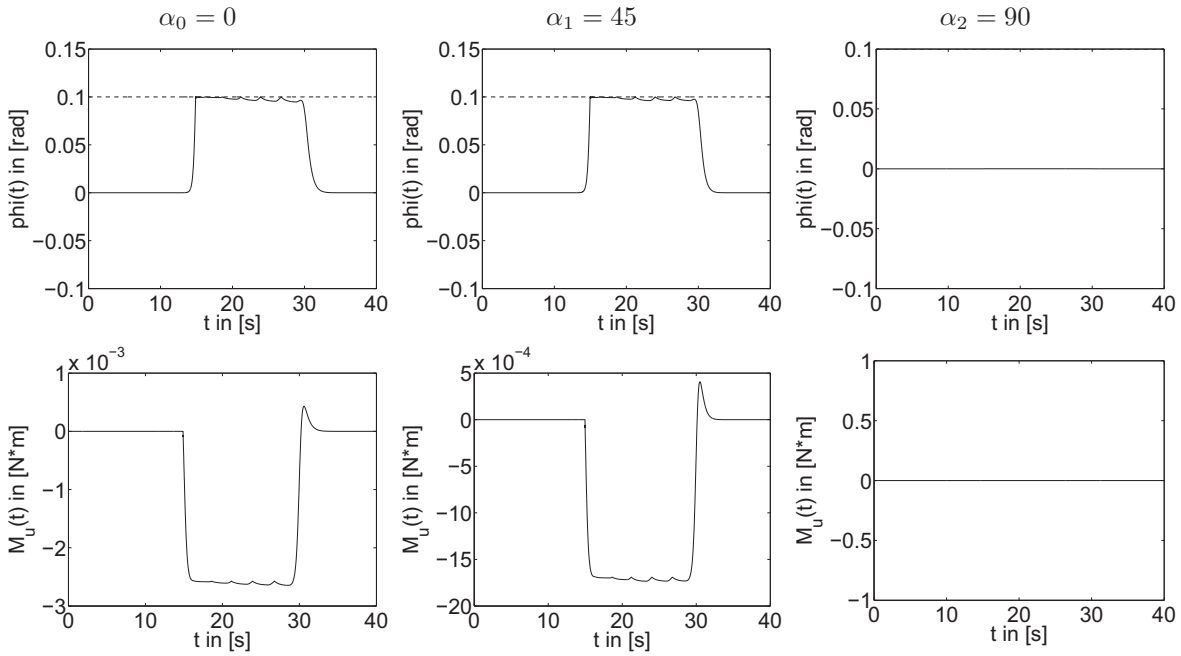

Fig. 16. **Model 2B: rotatory motion of the system in the passive mode**, deflected by an external force $\vec{F}_2$ with different angles of attack α.

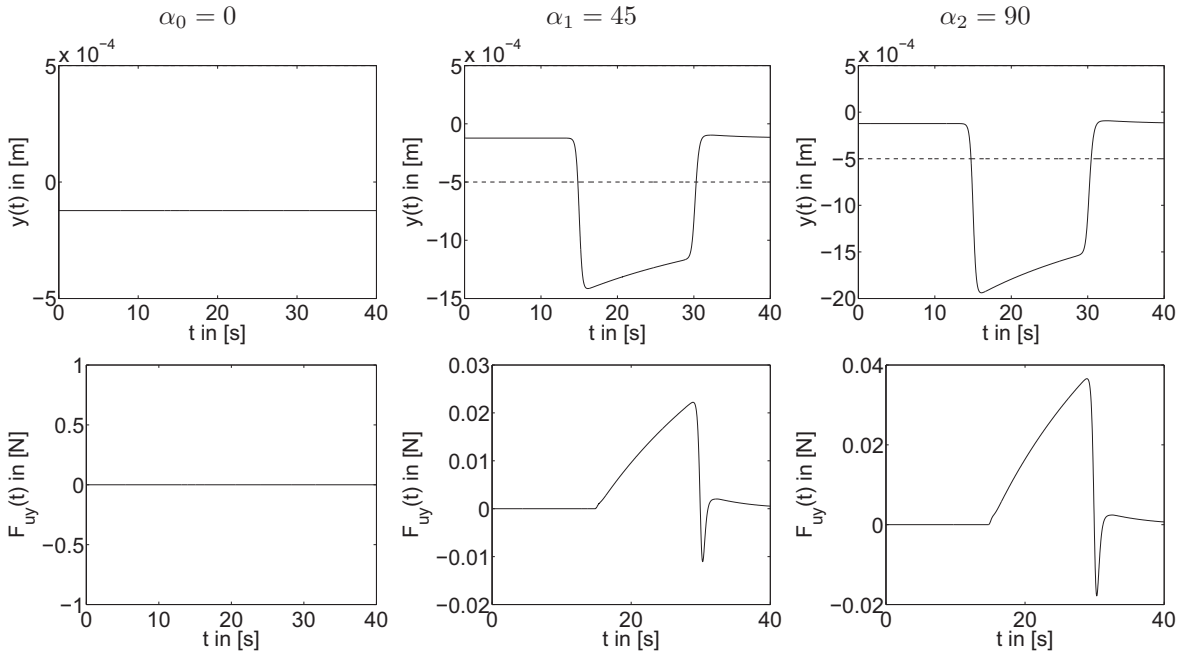

Fig. 17. **Model 2B: translatory motion of the system in the passive mode**, deflected by the external force $\vec{F}_2$ with different angles of attack α.

4.2.2. Active mode

The Figures 18 and 19 illustrate the systems reaction on the disturbing force (11) in the active mode. The plots of the rotational deflection are similar to the corresponding plots out of the simulations with model 1 (also see Fig. 14). The course of the torque provides a decent depiction of the acting force for angles of attack reaching from small to medium and can be used for the identification of the acting force. The statement about numerical errors caused by vertically acting forces ($\alpha = 90°$) made in the evaluation for model 1, may also apply here.

The graphs of the translatory displacement are identical to the corresponding graphs of the model in the passive mode. This can be seen as another evidence for the detachment between the translatory and rotatory motion of the rod. As described above, the graphs of the displacement $y(t)$ can be used for the identification of the external force in the active mode as well.

These observations were also made with the 1^{st} and 3^{rd} force (numerical simulations shown in [30]).

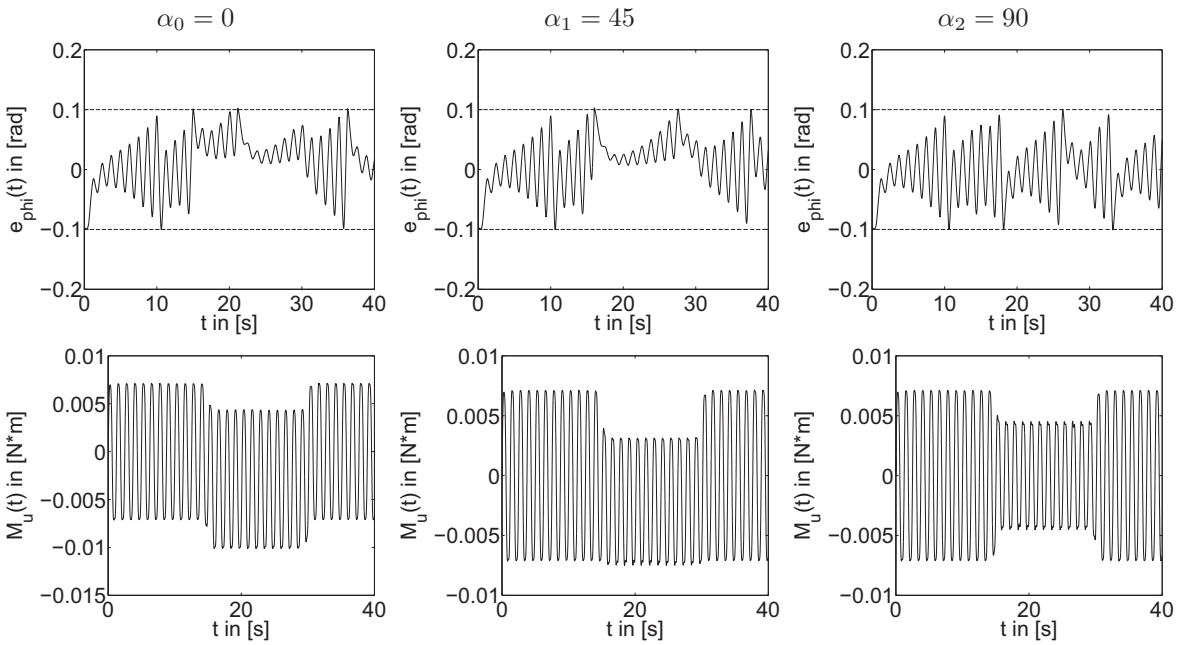

Fig. 18. **Model 2B: Rotatory motion of the system in the active mode** using the reference signal $\varphi_{ref1}(t)$ (exploratory whisking), deflected by the external force $\vec{F}_2$ with different angles of attack α.

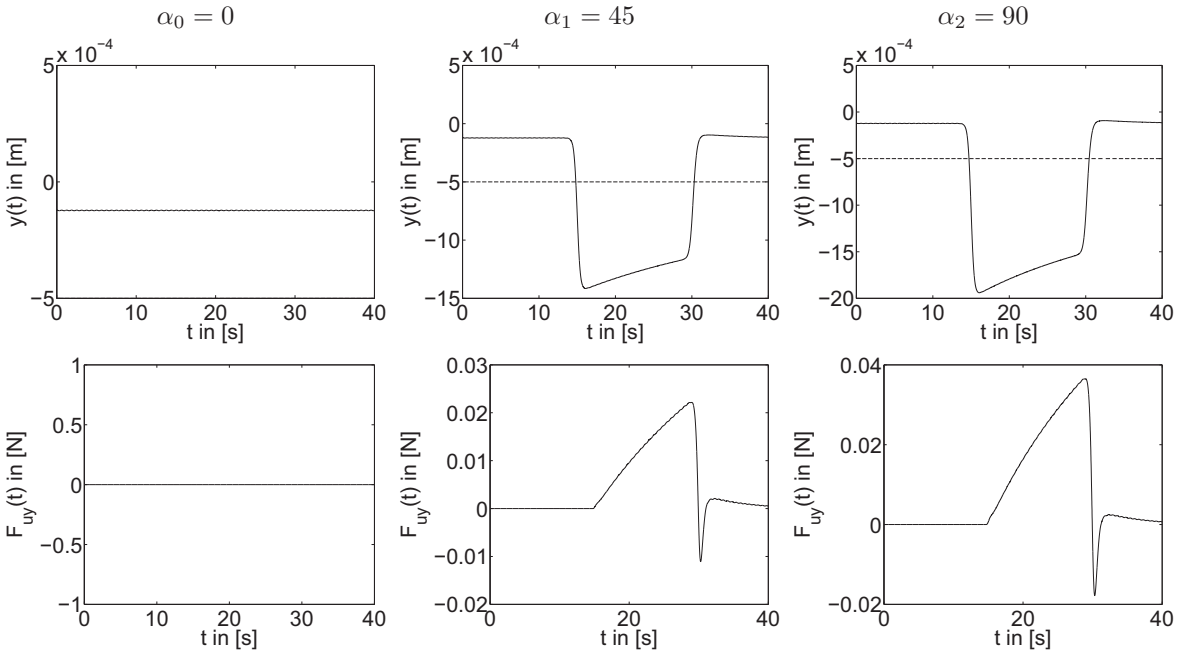

Fig. 19. **Model 2B: Translatory motion of the system in the aktive mode** using the reference signal $\varphi_{ref1}(t)$ (exploratory whisking), deflected by the external force $\vec{F}_2$ with different angles of attack α.

5. CONCLUSION

The examined mechanical models all meet the basic requirements for high-quality sensor systems:

- They react with sensitivity to occuring disturbance forces,
- the response time is short,
- the disturbance force can be identified.

Still the performance of the models differ greatly from another, especially in the latter point. The gradual increase of the degree of freedom from model 1 (DoF 1), to the models 2A, 2B (DoF 2) and 3 (DoF 3) revealed the significant benefits of the respective direction of motion. Thus, although the enhancement of model 1 with a translatory DoF in x-direction led to an improvement of the sensibility in model 2A (see [30]), the additional DoF in y-direction was by far more relevant for the identification of the disturbance force: in model 2B the force can be identified in the passive, as well as in the active mode – and this for angles of attack reaching from $0°$ to $90°$. Yet the positive characteristics of the models 2A and 2B could not be united in model 3: the interaction between the translatory displacement in x with the angular deflection φ impeded, especially in the active mode, the identification of the disturbance force.

While the models 1 and 2A are only suitable for applications with forces acting mostly horizontally, the models 2B and 3 can also provide reliable information in widely unknown surroundings. Furthermore, model 2B can be used in the passive, as well as in the active mode.

Future work shall be directed to elastic vibrissa systems modeled as a single beam.

6. ACKNOWLEDGEMENT

The authors thank Prof. rer. nat. habil. (em.) Joachim Steigenberger (Ilmenau) for fruitful discussions, hints and continuous interest.

References

[1] J. Doerfl, "The musculature of the mystacial vibrissae of the white mouse," *J. Anat.*, vol. 135, pp. 147–154, 1982.

[2] K. Carl, *Technische Biologie des Tasthaar-Sinnessystems als Gestaltungs- grundlage für taktile stiftführende Mechanosensoren*, Phdthesis, TU Ilmenau, 2008.

[3] R.W. Berg and D. Kleinfeld, "Rhythmic whisking by rat: Retraction as well as protraction of the vibrissae is under active muscular control," *Journal of Neurophysiology*, vol. 89, pp. 104–117, 2003.

[4] E. Ahissar, R. Sosnik, and S. Haidarliu, "Transformation from temporal to rate coding in a somatosensory thalamocortcal pathway," *Nature*, vol. 406, pp. 302–407, 2000.

[5] B. Mitchinson, M. Pearson, C. Melhuish, and T.J. Prescott, "A model of sensorimotor coordination in the rat whisker system," *From animals to animats 9: Proc. 9th. Int. Conf. on Simulation of Adaptive Behaviour*, vol. 4095, pp. 77–88, 2006.

[6] B. Mitchinson, C.J. Martin, R.A. Grant, and T.J. Prescott, "Feedback control in active sensing: rat exploratory whisking is modulated by environmental contact," *Proc. R. Soc. B*, vol. 274, pp. 1035–1041, 2007.

[7] Dori Derdikman, Chunxiu Yu, Sebastian Haidarliu, Knarik Bagdasarian, Amos Arieli, and Ehud Ahissar, "Layer-specific touch-dependent facilitation and depression in the somatosensory cortex during active whisking," *The Journal of Neuroscience*, vol. 26, no. 37, pp. 9358–9547, 2006.

[8] J.C. Curtis and D. Kleinfeld, "Seeing what the mouse sees with its vibrissae: A matter of behavioural state," *Neuron*, vol. 50(4), pp. 524–526, 2006.

[9] Erika E. Fanselow and Miguel A. L. Nicolelis, "Behavioral modulation of tactile responses in the rat somatosensor y system," *The Journal of Neuroscience*, vol. 19, no. 17, pp. 7603–7616, 1999.

[10] R.A. Russell, "Closing the sensor-computer-robot control loop," *Robotics Age*, vol. 6, pp. 15–20, 1984.

[11] T. Prescott, M. Pearson, B. Mitchinson, J. Sullivan, and A. Pipe, "Whisking with robots - from rat vibrissae to biomimetic technology for active touch," *IEEE Robotics and Automation Magazine*, vol. 16(3), pp. 42–50, 2009.

[12] D. Jung and A. Zelinsky, "Whisker based mobile robot navigation," in *Intelligent Robots and Systems '96, IROS 96, Proceedings of the 1996 IEEE/RSJ International Conference on*, 1996, vol. 2, pp. 497–504.

[13] A. Seth, J. McKinstry, G. Edelman, and J. Krichmar, "Texture discrimination by an autonomous mobile brain-based device with whiskers," in *Proceedings of the 2004 IEEE International Conference on Robotics & Automation*, 2004, pp. 4925–4930.

[14] M. Fend, S. Bovet, and H. Yokoi, "An active artificial whisker array for texture discrimination," in *Proceedings of 2003 IEEE/RSJ International Conference on Intelligent Robots and Systems*, 2003, pp. 1044–1049.

[15] H. Yokoi, M. Fend, and R. Pfeifer, "Development of a whisker sensor system and simulation of active whisking for agent navigation," in *Proceedings of 2004 IEEE/RSJ International Conference on Intelligent Robots and Systems*, 2004, pp. 607–612.

[16] M. Fend, "Whisker-based texture discrimination on a mobile robot," in *Proceedings of the 8th European Conference on Artificial Life (ECAL)*, 2005, pp. 302–311.

[17] S. N'Guyen, P. Pirim, and J.A. Meyer, "Tactile texture discrimination in the robot-rat psikharpax," *BIOSIGNALS 2010, 3rd Int Conf on Bio-Inspired Systems and Signal Processing*, 2010.

[18] A.E. Schultz, J.H. Solomon, M.A. Peshkin, and M.J. Hartmann, "Multifunctional whisker arrays for distance detection, terrain mapping, and object feature extraction," in *Proceedings of the 2005 IEEE International Conference on Robotics and Automation*, 2005, pp. 2588–2593.

[19] B. Mitchinson, K.N. Gurney, P. Redgrave, C. Melhuish, A.G. Pipe, M. Pearson, I Gilhespy, and T.J. Prescott, "Empirically inspired simulated electro-mechanical model of the rat mystacial follicle-sinus complex," *Proc. R. Soc. Lond.*, vol. 271, pp. 2509–2516, 2004.

[20] D. Hill, R. Bermejo, P. Zeigler, and D. Kleinfeld, "Biomechanics of the vibrissa motor plant in rat: Rhythmic whisking consists of triphasic neuromuscular activity," *The Journal of Neuroscience*, vol. 28, pp. 3438–3455, 2008.

[21] C. Behn, *Ein Beitrag zur adaptiven Regelung technischer Systeme nach biologischem Vorbild*, Phdthesis, TU Ilmenau, 2005.

[22] C. Behn, J. Steigenberger, and K. Zimmermann, "Finite degree-of-freedom models for animal vibrissae," *ECC 2009,Budapest*, pp. 2500–2505, 2009.

[23] C. Behn and J. Steigenberger, *Improved Adaptive Controllers For Sensory Systems - First Attempts, in Modeling, Simulation and Control of Nonlinear Engineering Dynamical Systems*, Number ISBN 978-1-4020-8777-6. Springer, 2009.

[24] T. Schmitz, "Modellbildung des reizleitungsapparates am beispiel vibrisse und adaptive regelungsprozesse," Bachelorthesis, TU Ilmenau, 2009.

[25] J. Dudel, R. Menzel, and R.F. Schmidt, *Neurowissenschaft - Vom Molekül zur Kognition*, Springer, 1996.

[26] C. Behn and J. Steigenberger, "Bio-inspired adaptively controlled mechanical vibrissae," *GAMM Tagung 2009, Danzig, Polen*, 2009.

[27] V. Gopal and M. Hartmann, "Using hardware models to quantify sensory data acquisition across the rat vibrissal array," *Bioninspiration & Biomimetics*, vol. 2, pp. 135–145, 2007.

[28] M. Stüttgen, S. Kullmann, and C. Schwarz, "Responses of rat trigeminal ganglion neurons to longitudinal whisker stimulation," *The Journal of Neurophysiology*, vol. 100, pp. 1879–1884, 2008.

[29] M.A. Neimark, M.L. Andermann, J.J. Hopfield, and C.I. Moore, "Vibrissa resonance as a transduction mechanism for tactile encoding," *The Journal of Neuroscience*, vol. 23(16), pp. 6499–6509, 2003.

[30] T. Schmitz, “Entwurf und analyse von biologisch inspirierten sensorsystemen mit erhöhtem freiheitsgrad am beispiel vibrisse,” Mastersthesis, TU Ilmenau, 2011.

[31] MATLAB, “Product help: Function reference ”cos”,” 2008.